

Fabrication of aerogels from cellulose nanofibril grafted with β-cyclodextrin for capture of water pollutants

Diego Gomez-Maldonado¹ · Autumn Marie Reynolds¹ · Leena-Sisko Johansson² · Daniel J. Burnett³ · Jayachandra Babu Ramapuram⁴ · Matthew Neal Waters⁵ · Iris Beatriz Vega Erramuspe¹ · Maria Soledad Peresin¹

Accepted: 9 June 2021 / Published online: 2 July 2021 © The Author(s), under exclusive licence to Springer Science+Business Media, LLC, part of Springer Nature 2021

Abstract

Interactions at the molecular and surface chemistry are some of the key factors that determine the adsorption capacity of pollutants and emerging contaminants in porous materials. As filtration-based purification of water sources expands, the generation of green materials, such as biopolymers, is the priority. However, to increase the removal capacity, modification of natural polymers appears necessary. Nanomaterials, especially bio-based materials like cellulose nanofibrils, inherently have large surface areas as a consequence of their high aspect ratios. Their capacity to modulate the interactions with contaminants present in water can be modulated by incorporating selective active points, such as hydrophobic cavities, that can further improve their overall adsorption capability. A bio-based material that can fulfil this requirement is β -cyclodextrin, a cyclic oligosaccharide with seven glucose units, which provides an easy grafting strategy onto cellulose due to structural affinity. Another advantage of using cellulose nanofibril is their film formability, aerogels, and hydrogels without the need of harsh chemicals or processes. In this work, an oligosaccharide with a hydrophobic centre – β -cyclodextrin – was immobilized onto bleached softwood cellulose nanofibrils, and then used to generate high surface area aerogels with a density of 175 kg/m³ and porosities above 88%. Charge density titration, Fourier transform infrared with attenuated total reflectance (FTIR-ATR), X-ray photoelectron spectroscopy (XPS), thermogravimetric analysis (TGA), and atomic force microscopy (AFM) characterization techniques were used to assess the successful modification of the fibrils. Inductive coupled plasma mass spectroscopy (ICP-MS) was used to determine the lack of trace chlorine in the material from the grafting process while scanning electron microscopy (SEM) and dynamic vapor sorption (DVS) were used to determine porosity and surface area of the aerogels. The adsorption capacity was tested with two molecules of different natures: a cyanotoxin (microcystin-LR) and a dye (methylene blue), using high-performance liquid chromatography with a UV detector (HPLC-UV) and UV-vis spectroscopy, respectively. The adsorption in equilibrium for CNF-CD aerogels was calculated to be 0.078 mg/g of microcystin-LR and 3.46 mg/g of methylene blue, enlightening its possible use to improve water quality.

 $\label{eq:continuous} \textbf{Keywords} \ \ Cellulose \ nanofibril \cdot \beta \text{-cyclodextrin} \cdot Aerogels \cdot Water \ remediation \cdot Physical \ adsorption \cdot Microcystin-LR \cdot Methylene \ blue$

- Maria Soledad Peresin soledad.peresin@auburn.edu
- Forest Products Development Center, School of Forestry and Wildlife Science, Auburn University, Auburn, AL 36849, USA
- Department of Bioprocesses and Biosystems, School of Chemical Engineering, Aalto University, 00076 Aalto, Finland
- Surface Measurement Systems, Allentown, PA 18103, USA
- ⁴ Harrison School of Pharmacy, Auburn University, Auburn, AL 36849, USA
- Department of Crop, Soil and Environmental Sciences, Auburn University, Auburn, AL 36849, USA

1 Introduction

As clean water sources are negatively impacted by increasing industrial and agricultural activities and global urbanization, there is a rising need to develop low-cost, renewable, and widely available sorbents that can be used to increase water quality [1–3]. The efficiency of these sorbents is linked to the material surface chemistry and surface area as well as the possible molecular interactions between the material and the given pollutants [4–6].

When selecting materials for the development of filtration sorbents, worldwide efforts to lower carbon emissions



need to be taken into consideration. These efforts have prompted the development of green materials and processing technologies that aim at replacing widely used fossil fuel-derived analogues. Along these lines, the utilization of bio-based materials to develop sorbents for water treatment is of particular interest [7–14]. Out of various bio-based materials, cellulose nanofibrils (CNF) is considered a versatile substrate due to their wide availability, well-established structures, and chemical reactivity, allowing for their modification to target specific interactions towards particular pollutants of interest [15–17]. Cellulose, as a molecule, is a polysaccharide made of β -(14) glucopyranoside units with chain conformations that vary in length and crystalline structure from organism to organism. Cellulose chains are organized in highly packed bundles by intra- and intermolecular hydrogen bonds, which interact with the additional plant cell wall components that conform to the so-called lignocellulosic materials [18, 19]. Lignocellulosic materials can be treated by chemical, mechanical, or enzymatic ways to produce cellulose fibers in dimensions that can vary from the micro to the nanoscale [20]. In particular, CNF present characteristic high surface area along with inherent biocompatibility, high mechanical strength, and light weight which make them highly suitable for a range of applications, including water treatment applications [21-23]. In particular, CNFs can be assembled into 3-D structures that not only maintain a high surface area but also provide dimensional stability so they can be further manipulated, such as highly porous and low-density aerogels [24, 25].

Cellulose nanomaterials have been proven to adsorb positively charged pollutants like metallic ions [26, 27] or polypeptides [28, 29]. These interactions are mainly driven by electrostatic or van der Waals interactions, which increase the total entropy of the systems by liberating adsorbed water [30]. This is highly appealing as the capturing of a wide variety of pollutants is driven by these same mechanisms. In addition to this, multiple emerging contaminants such as dyes, aromatics, or hydrocarbons are complex molecules for which their adsorption on the sorbent could be benefited by the addition of hydrophobic active points on the cellulose nanofibril surface, with straightforward routs such as grafting of β -cyclodextrin. β -cyclodextrin has been shown to improve the adsorption of pollutants when was grafted onto magnetic graphene sheets and porous silica [31], chitosan/graphene sheets [32], carbonaceous nanofibrils [33], biomass/polysulfone/polyethylenimine [34], and cellulosebased materials [35–39].

However, the formation of aerogels with pre-grafted cellulose nanofibril has not been widely explored. The potential impact of this approach on the adsorption of organic pollutants is intriguing and holds great potential for removal of such pollutants and for increasing water quality.

In this work, bleached softwood cellulose nanofibrils (CNF) were crosslinked with β -cyclodextrin (CD) via epichlorohydrin, and aerogels were formed from this material by solvent exchange (ethanol and tert-butanol), followed by freeze-drying. Charge density titration, Fourier transform infrared with attenuated total reflectance (FTIR-ATR), X-ray photoelectron spectroscopy (XPS), thermogravimetric analysis (TGA), and atomic force microscopy (AFM) characterization techniques were used to confirm the modification of the fibrils; inductively coupled plasma optical emission spectroscopy (ICP-OES) was used to monitor traces of chlorine after grafting reaction. Scanning electron microscopy (SEM) and dynamic vapor sorption (DVS) were used to determine the surface area and surface energy of the aerogel. For testing adsorption capability, two different target molecules were chosen: a cyclic oligopeptide with a prominent hydrophobic residue: microcystin-LR- (a cyanotoxin) and methylene blue (a commonly used cationic dye) to elucidate preferred adsorption mechanisms between pristine CNF and the CNF grafted with β-cyclodextrin (CNF-CD). The adsorption of microcystin-LR was followed by high-performance liquid chromatography with an UV detector (HPLC-UV), while UV-Vis spectroscopy (UV-Vis) was the chosen analytical tool to monitor the adsorption of methylene blue. A schematic flowline of this paper can be found in Scheme 1.

2 Experimental

2.1 Materials

Bleached cellulose nanofibrils (2.76%, pH 6.3) were produced at the Forest Products Development Center at Auburn University from bleached pulp from mixed softwood kindly provided by a North American papermill; β-cyclodextrin (>98%, CD) was purchased from Tokyo Chemical Industry America (Portland, OR, U.S.); epichlorohydrin (99%, EPI) was obtained from Acros Organics (Geel, Belgium); microcystin-LR (>95%, MC) from Cayman Chemicals (Ann Arbor, MI, U.S.); methylene blue and 2,4-dichlorophenol were purchased from Merck KGaA (Darmstadt, Germany); hydrochloric acid (37.6% solution) purchased from Fisher Scientific (Waltham, MA, U.S.); sodium hydroxide (50% w/w solution) purchased from J.T. Baker (Phillipsburg, NJ, U.S.); ammonium hydroxide (18-30% solution) purchased from VWR International, LLC., (Radnor, PA, U.S.); ethanol (200 proof pure) purchased from Decon Labs, Inc. (King of Prussia, PA, U.S.); and tert-butanol (>99%) was acquired from Sigma-Aldrich Co., (San Luis, MO, U.S.). The water



Scheme 1 Schematic outline of Aerogel formation of Synthetize this work CNF-CD / CNF In vitro capturing tests CNF-CD via solvent exchange via Epichlorohydrin crosslinking (etOH & tertbutanol) XPS SEM HPLC-UV Charge Density **AFM** DSV UV-Vis FTIR ICP-MS Swelling TGA

used was deionized and purified with a Thermo Scientific Barnstead nanopure (18.2 m Ω cm).

2.2 Cellulose nanofibrils (CNF) production

For the preparation of the CNF solution, the bleached pulp was diluted to a 2% wt. suspension. Washing was done as pre-treatment of the pulp to eliminate residual metals and another component. The washing consisted in first lowering the pH to 3 with a 1 M HCl solution; after 30 min washings of the pulp were done with DI water until pH increased to 4.5–5, then NaHCO₃ was added to obtain a 0.001 M concentration, and pH was adjusted to 9 with 1 M NaOH. After 30 min, washings were performed until no changes in conductivity were measurable. Finally, the washed pulp was then processed by Masuko super mass colloider (MKZA-10-15 J) for 20 passes, with a final consistency of 2.76% wt. at a pH of 6.3.

2.3 Synthesis of crosslinked cellulose nanofibrils/ β-cyclodextrin (CNF-CD)

A low concentration solution of CNF was prepared (625 mL, 0.004% w/v) and left overnight stirring at 4 °C. Then, 75 mL of 40% v/v NaOH was mixed with 12.5 g β-cyclodextrin. Once dissolved, the solution was added to the CNF solution and stirred for one hour. The temperature was then raised to 65 °C in a water bath. In the meantime, 38 mL of epichlorohydrin were added dropwise to obtain a final ratio of (1:5:25 mol of CNF:CD:EPI). The solution was left to react for 2 h while stirring at 160 rpm. After cooling to room temperature, the solution was vacuum filtered with a PYREX Buchner funnel (using Whatman TM glass microfiber filters diameter 70 mm Cat No. 1820–070) until the cake released no more water. After removal, the material was put in an extraction glass fibre thimble inside a Soxhlet

extractor system with 375 mL of acetone at 80 $^{\circ}$ C and left for 16 cycles. The material produced was then re-suspended in 375 mL of ultrapure water and neutralized to a pH of 7.03 with 1 M HCl. Once neutralized, the CNF-CD solution was vacuum filtrated and stored at 4 $^{\circ}$ C.

2.4 Aerogels formation

CNF and CNF-CD were resuspended in ultrapure water to a 0.35% wt. consistency. From these solutions, 21 mL were vacuum filtrated in a filtration system assembled with a diameter of 25 mm with glass fibre filter paper. The filtration was done until a cake of approximately 1 cm was obtained, which was then transferred to a Teflon film (1.6 mm of thickness, 4 cm diameter) inside 6 cm petri dishes. A total of seven solvent changes were done, four in ethanol and three changes with tert-butanol with 15 mL steps and waiting times of 1 h before the next change. After the last removal of tert-butanol, the filtrated cakes were frozen and freezedried in a Freezone 12 (Labconco, Kansas City, MO, U.S.).

2.5 Characterization techniques

2.5.1 Charge density

Charge densities of the CNF, CNF-CD and CD were measured using a method adapted from Espinosa et al. [40]. Measurements were repeated 6 times and averaged. In brief, suspensions with 0.04% wt. consistency were prepared and pH was adjusted to 6.5 for both solutions using 1 M HCl or NaOH. 15 mL of this suspension were mixed with 25 mL of pDADMAC and centrifuged at 3000 rpm for 15 min. After centrifugation, 10 mL of the supernatant were separated and analyzed using a Laboratory Charge Analyzer Chemtrac LCA-1, (Norcross, GA). For this analysis, the solution was titrated with PSVK until the equipment reached 0 streaming



current value (SCV). The volume of titrant consumed was used for the final calculations using the following equation (Eq. 1)

where Polydiallyldimethylammonium chloride [pDADMAC] is the concentration of the cationic polymer, $V_{p\text{-}DADMAC}$ is the used volume of p-DADMAC, potassium polyvinylsulfate [PVSK] is the concentration of the anionic titrant, V_{PVSK} is the consumed volume of titrant, and $W_{dry\ sample}$ is the weight of the dry CNF, CNF-CD or CD sample.

2.5.2 Fourier-transform infrared spectroscopy with attenuated total reflectance

Air-dried samples were analyzed to characterize the surface modification using a PerkinElmer Spotlight 400 FT-IR Imaging System (Waltham, MA, US) with an ATR accessory with diamond/ZnSe crystal and a resolution of 4 cm⁻¹. First, a background spectrum with the clean sensor was measured; this was carried-out before each set of measurements with the same number of scans. To archive a high resolution at the spectrum bands, 512 scans per spectrum were performed. Data was processed with Spectrum 6 Spectroscopy Software (PerkinElmer, Massachusetts, US).

2.5.3 X-ray photoelectron spectroscopy

Surfaces of the CNF and CNF-CD were mounted on an XPS sample holder using UHV compatible carbon tape. The chamber with the samples and a piece of pure cellulose -as the in-situ reference monitoring analysis conditions during the measurement [41]- were pre-evacuated overnight together. The gathered data were recorded using monochromatic Al Kα irradiation at only 100 W and under neutralization. For the data analysis, high-resolution C 1 s regions were fitted with Gaussian components of equal half widths, and the binding energies of all spectra were charge-corrected using the main component of cellulose, namely C–O at 286.7 eV, as the binding energy reference [42].

2.5.4 Thermogravimetric analysis

Air-dried samples were tested on aluminium pans in a TGA-50 from Shimadzu (Kyoto, Japan). Samples were heated from room temperature to 600 °C at a rate of 10 °C/min under a nitrogen atmosphere and data was processed with TA60 software version 2.11 from Shimadzu.



2.5.5 Atomic force microscopy

Surface characterization of the CNF and CNF-CD were done in spin-coated silicon wafers (2×2 cm², with 180 µL of ca. 0.01% material at 3000 rpm for 1 min) using a Tosca 400 equipment from Anton-Paar (Gratz, At). Height images were obtained by tapping mode with a NanoWorld (Neuchâtel, Switzerland) ARROW-NCR-20 silicon SPM-sensor cantilever with a resonance frequency of 285 kHz and constant force of 42 N/m; scan sizes were 5×5 µm² and 10×10 µm². Processing of the images was done with Gwyddion software 2.49 (SourceForge) and roughness calculations were done with ProfilmOnline (KLA Corporation, Milpitas, CA, U.S.).

2.5.6 Inductive coupled plasma optical emission spectroscopy

Samples of CNF and CNF-CD were analysed for chloride concentrations using a Thermo Electron iCAP-RQ inductively coupled plasma mass spectrometer (ICP-MS, Thermo Fisher Scientific) per Standard Method 3125-B [43]. Samples and calibration standards were prepared in a matrix of 2% nitric acid by volume.

2.5.7 Scanning electron microscopy

Freeze-dried CNF and CNF-CD aerogels were placed on aluminium studs and sputtered with gold for 60 s in a Q150R ES sputter coating device acquired from Electron Microscopy Sciences (Hatfield, PA, U.S.). Images were recorded using 20 kW, working distance between 6 and 8 mm and with a magnification of 1000X in a Zeiss Evo 50VP scanning electron microscope (Oberkochen, Germany).

2.5.8 Dynamic vapor sorption

For all experiments, approximately 125 mg of each aerogel were packed into individual silanized glass columns (300 mm long by 4 mm inner diameter) using the SMS Column Packing Accessory. Each column was conditioned for a period of 2 h at 30 °C and 0% RH with helium gas prior to any measurements. All experiments were conducted at 30 °C with 25 sccm total flow rate of helium gas, using methane for dead volume corrections. Samples were run at a series of surface coverages with n-alkanes (nonane, octane, heptane, and hexane; Aldrich, HPLC grade) and polar probe molecules (acetone, ethanol, acetonitrile, ethyl acetate, and dichloromethane; Aldrich, HPLC grade) to determine the dispersive surface energy as well as the specific free energies of adsorption, respectively. The complete IGC experiment overall surface coverages measured took approximately 24 h for one sample. Repeat experiments were completed in succession on the same column to investigate if the elapsed time or exposure to vapours caused any measurable surface changes. Dispersive surface energy values were repeatable within \pm 1.0 mJ/m² and acid-base surface energy values were repeatable within \pm 0.5 mJ/m². All surface energy analyses were carried out using iGC Surface Energy Analyzer (SMS, Alperton, UK) and the data were analyzed using both standard and advanced SEA Analysis Software.

2.5.9 Water uptake and swelling

To calculate water uptake, the dried aerogels were immersed in 20 mL of ultrapure water, from which they were removed at regular time intervals up to 240 min and weighted. The averaged results for water uptake were calculated by the following equation (Eq. 2).

Water uptake (%) =
$$\frac{Wt - Wd}{Wd} \times 100$$
 (2)

where Wt is the weighted mass, and Wd is the dry weight of the aerogels. Meanwhile, for the swelling, the aerogels were left for 24 h in 20 mL of ultrapure water before weighting. The average results were then calculated with the next equation (Eq. 3).

Swelling (%) =
$$\frac{Ws}{Wd} \times 100$$
 (3)

where Ws is the weight obtain after swelling.

2.5.10 Density and porosity

Dimensional measurement of the aerogels was done using a digital caliper and used to calculate volume and density (ρ_a) . The porosity was obtained by equation (Eq. 4), where the density of the cellulose (ρ_c) was assumed to be 1460 kg/m³, as reported in the literature [25].

$$Porosity (\%) = 1 - \frac{\rho_a}{\rho_c} \times 100 \tag{4}$$

2.6 Adsorption experiments

2.6.1 High-pressure liquid chromatography

For the analysis of microcystin, the aerogels were placed in 20 mL of solutions containing 1.5 and 0.8 μ g/mL at room temperature and constant stirring. 150 μ L aliquots were taken at the corresponding time and analyzed in a Waters Alliance HPLC (Model No. e2695, Waters Corp., Milford, MA, USA) system equipped with a solvent management system 2695 and detected by a photodiode array detector (PDA, 2998). The system also counts with a thermostatically controlled column compartment and an autosampler. The

method used was adapted from the one described by Meriluoto & Spoof [44]. Briefly, a C-18 column ($150 \times 4.6 \text{ mm}^2$) was used as stationary phase, and 0.05% trifluoroacetic acid (TFA) aqueous solution/0.05% TFA acetonitrile with a linear gradient at a flow rate of 1 mL/min, and 10 μ L injections using the autosampler in cycles of 9 min. The retention time was 4.2 min, and the correlation coefficient (r) of the samples to the standard curve was of 0.9997. All experiments were done by triplicates and averaged. The analysis of the data was performed using Empower® 3 software (Waters Corp.).

2.6.2 UV-Vis spectroscopy

All absorbance data was collected in a SpectraMax M2 from Molecular Devices (Silicon Valley, CA, USA) and data was visualized on the software SoftMax Pro 6.5.1. For methylene blue adsorption and desorption experiments, filters were immersed in 50 mL of a 15 mg/L solution and kept at 25 °C with constant stirring; absorbance measurements were done at λ = 664 nm. All experiments were done by triplicated and averaged.

2.6.3 Kinetics

The fitting of the data to calculate rate constants $(k_1 \text{ and } k_2)$ and adsorbed amounts in equilibrium (qe) was done for a pseudo-first-order and pseudo-second-order models when possible following the equations given in [45]. Briefly, for pseudo-first-order:

$$ln (qe - qt) = ln qe - k_1 t$$
(5)

For pseudo-second order:

$$\frac{t}{qt} = \frac{1}{h} + \frac{t}{qe} \tag{6}$$

where $h = k_2 qe^2$, with k_1 and k_2 being the pseudo-first and pseudo-second order rate constant of sorption, respectively. qe is the amount of analyte adsorbed at equilibrium (mg/g), and qt is the amount of analyte adsorbed at any time (mg/g).

The linear plots for the pseudo-second order were first done to obtain qe and h, and the obtained qe was used for the pseudo-first order when possible, for the fitting.

3 Results and discussion

3.1 Synthesis of CNF-CD

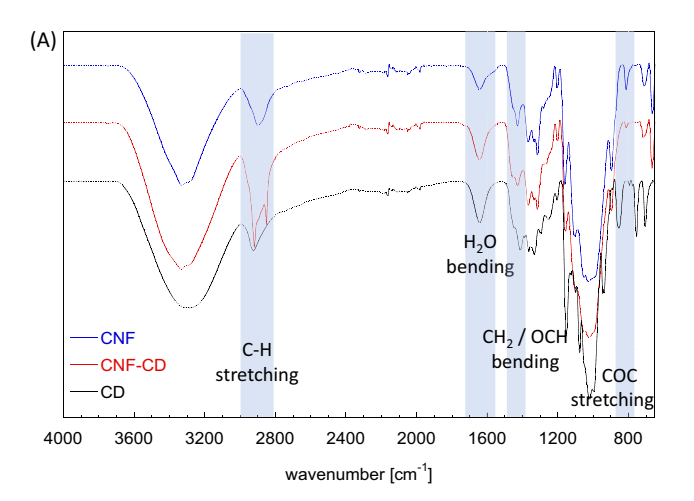
The success of the grafting reaction was followed by a combination of analytical techniques. Comparing the charge densities (see Table 1) of pristine CNF and CNF-CD, the



Table 1 Charge density values of the different elements used

Sample	Charge density [µeq/g]	St. Dev	pН
CNF	- 126.67	64.89	6.5
CNF-CD	-202.22	48.57	6.5

CD-grafted CNF shows a drop of 37.4% compared to the initial negative charge density of the pristine CNF, with means statistically different (Figure S1). This increase can be related to an increase of functional groups as a side reaction of the grafting in alkaline conditions [46], or by the formation of aldehyde and other ionizable groups with the



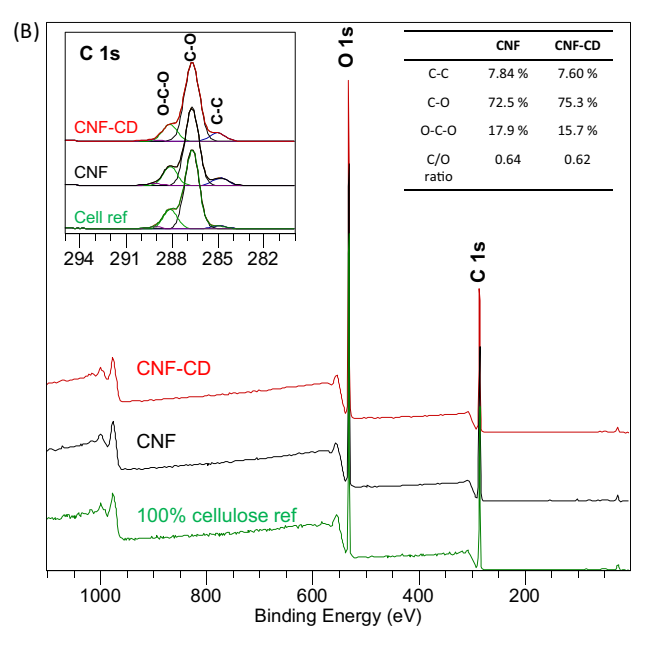
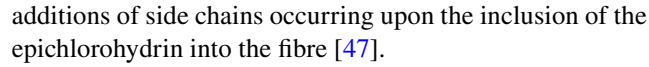


Fig. 1 Chemical comparison of the used cellulose nanofibrils (CNF), β -cyclodextrin (CD), and the crosslinked CNF-CD. **a** FTIR spectra; **b** XPS wide energy region spectra and inserts showing the high-resolution C 1S spectra and the elemental data



When analysing FTIR spectra (shown in Fig. 1a), changes in the C-H stretching band (2900 cm⁻¹) are perceptible in the CNF-CD; due to the introduction of aliphatic CH₂ with the molecular bridges, the product of the crosslinking via EPI [47, 48]. These bonds can also be seen in the changes in the bands related to OCH/CH₂ bending at 1423 cm⁻¹, where it can be observed that the main band decreases and the shoulder is more defined. Finally, the band at 1640 cm⁻¹ is traditionally related to the adsorbed water. In this band, the shoulder that is present in the CNF spectrum increases in intensity for the crosslinked polymer, which reveals a greater similarity of the CNF-CD to the CD spectrum, showing the presence of these components in the conjugated system.

These changes can also be observed in the XPS wide energy region and the high-resolution C 1 s spectra (Fig. 1b), where there is a 2.8% increase in the C-O bonds in the surface from the pristine CNF to the modified CNF-CD. There it can also be seen a reduction in the proportion of O-C-O bonds with a 2.2% decrease, that indicates the introduction of covalent bonds related to the induced bridges formed by the EPI connecting the cellulose and cyclodextrin. In other words, the decrease can be explained due to the presence of more aliphatic carbons on the surfaces, which translates to a lower proportion of the O-C-O signal coming from the cyclic ring than the monomers. Moreover, a decrease in the C/O ratio was observed from 0.64 to 0.62, further confirming the modification of the fibres. However, as the epoxy chemistry pathway uses aleatory hydroxyl groups as crosslinking points, the increase in the C-O cannot be directly translated to a degree of functionalization.

Alternatively, thermal analysis of the samples was conducted to collect additional evidence of the chemical

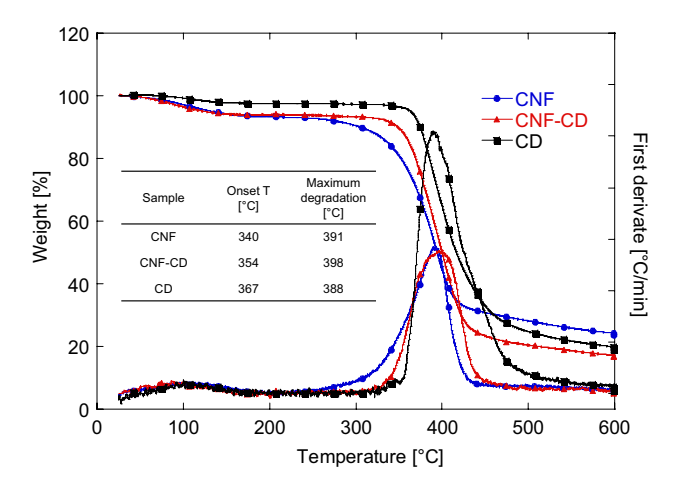


Fig. 2 Thermograms comparing the used cellulose nanofibrils (CNF), β -cyclodextrin (CD) and inserts of the first derivate and the main thermal degradation data



modification using TGA. Thermograms can be found in Fig. 2. From these tests, it can be observed that the grafting of the CD increased the onset temperature of the modified CNF, however keeping it lower than the free CD. These results are in accordance with other cellulose and cyclodextrin systems found in the literature [49]. However, in this work, the addition of the cyclodextrin to the CNF increased the max degradation temperature, as more packing of the fibres is present [50]; which also can be confirmed with the AFM images presented in Fig. 3.

When analyzing the morphology of the surfaces using AFM (Fig. 3), the mean rugosity root square height (Rsq) of the grafted fibers showed an increment of 49% on respect of the pristine CNF. Such rugosity increase could be related to the additional bonding created between CNF fibrils and cyclodextrin molecules. This also correlates with a perceptibly increased thickness on the fibers and the more granular appearance of the surface. No traces of chloride were found in either the CNF or the CNF-CD as revealed by ICP-MS (Table S1), assuring that its use for applications such as water remediation would not be jeopardized by the crosslinking methodology, as not extra pollutants -such as chloride- could leach from this system.

3.2 Aerogel formation

The first observable difference between the aerogels was visible after freeze-drying, there the pristine CNF lost more height than the modified fibres, suggesting that the dragging forces were strong enough to induce hornification on the cellulose fibrils due to the larger hydrogen bonding and hydration present in the unmodified systems [51]. However, this phenomenon is not as clear for the CNF-CD, probably related to the observed increase in diameter and rugosity after modification, as the hydroxyl groups were used during the immobilization decreasing the ability of water to coalesce the fibrils.

Fig. 3 Tapping mode AFM images of CNF (left) and CNF-CD (right) spin-coated surfaces

Physical properties of the aerogels are listed in Table 2. Further differences between the two aerogels are presented there; for example, it can be observed that the modified aerogels presented 20% more weight than the aerogels formed from only CNF. This is important as the total dry mass used for the formation of both types of aerogels was 73.5 mg, showing that the CNF lost more fibril fines during the vacuum-filtration than the crosslinked material, further confirming the difference in the diameter of the fibrils as observed by the increase in the rugosity values (Rsq) obtained from the AFM images (Fig. 3). The density values obtained also correlate to these observations, as the CNF-CD aerogels were 84% denser, which consequently presented a porosity decrease of 5.8% compared with the pure CNF. Additionally, the BET of the freshly prepared aerogels revealed a surface area 30% lower for CNF-CD, which can likewise be linked to the lower porosity and increase of thickness of the fibrils after the reaction. Additionally, the images obtained by SEM also present these visible differences between the two materials, where a more packed surface is also observed, even when the height of the aerogels formed from the CNF-CD were higher.

All the differences found between the two materials could then be tracked down to the modification of the fibrils. Which in turns indicates that, if lighter or less dense materials are desire, a finer control during the reaction would be needed to avoid undesired crosslinking between the fibrils.

Figure 4a shows the total surface energy profile of the aerogels obtained from DVS tests. The modified CNF-CD shows a significant lower surface energy, as expected by the presence of the β -cyclodextrin hydrophobic cavities and the aliphatic extensions contributed by the epichlorohydrin. When comparing wettability of the pristine CNF and CNF-CD (Fig. 4b), a higher wettability profile is observed for the later. Wettability is defined as the ratio between the acid–base surface component and the total surface energy of the material. A higher wettability for CNF-CD was expected, which correlates with the higher charge density of the

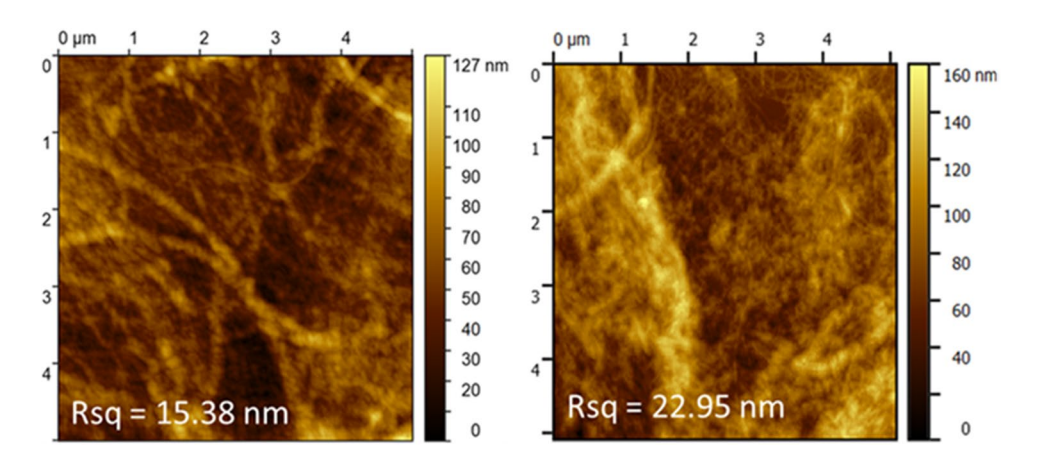




Table 2 Physical properties of the CNF and CNF-CD aerogels

Property	CNF aerogel	CNF-CD aerogel
Mass [mg]	54 .0±2.0	65.0±9.6
Density [kg/m ³]	95.0 ± 21	175 ± 49
Porosity [%]	93.4 ± 1.4	88.0 ± 3.3
BET surface area [m ² /g]	10.4	7.24
Total surface energy [mJ/m ²] (min, max)	(59.4, 74.9)	(50.6, 60.6)
Dry aerogel	AUBURN UNIVBRSITE	AUBURN UNIVERSITY
SEM images 1000x	20 µm/	20 μm

modified fibrils when compared to pristine CNF. However, wettability analysis only takes into consideration the possible acid—base contributions, while the total energy considers also additional dispersive forces, which allow H-bonding and van der Waals interactions to take place between the substrate and the molecules present in the media. Finally, the swelling capacity and water uptake was also higher for the CNF-CD with a 60% water uptake and 1200% swelling capacity compared to 50% and 800% for the aerogels obtained with CNF alone (Fig. 4c and 4d).

3.3 Molecular interactions

As previously discussed, interactions between pristine CNF and CNF-CD fibrils and water were significantly different. Thus, similar effects are expected upon interaction with pollutants. When comparing the microcystin-LR (MC) kinetics of adsorption on CNF at different concentrations (Fig. 5), CNF showed negative results in both cases. This is most likely due to the adsorption of water from the solution rather than MC adsorption. As a result, a higher concentration of microcystin in the remaining solution is expected. On the other hand, the microcystin adsorption on CNF-CD showed a maximum at 180 min with 0.043 mg MC/g of filter for the

solution with 0.8 µg/mL and 0.097 mg MC/g of filter in the 1.5 µg/mL solution. This translates to a removal capacity of 20.5% and 18.4% of the total toxin in the solution (Fig. 5b), respectively. However, adsorption decreased at longer monitored times, suggesting a reversible process driven by the interactions of water with the other residues from the amino acids present in the structure, as well as water interactions with the hydroxyl groups on the edge of the cyclodextrin structure [52]. When the adsorption was analysed using a pseudo-second-order fitting (Table 3), the equilibrium adsorption capacity (qe) was calculated to 0.078 mg/g and 0.034 mg/g for each concentration, respectively. These results from the fitting are like the values observed during the first minutes after the beginning of the interaction. This could imply that the interaction between the hydrophobic cavities and the targeted molecule occur rapidly, suggesting then that the rest of the adsorption observed could be mostly driven by some weak interactions (probably van der Waals) that are later lost as the water interacts with the surface of the sorbent and the more polar residues of the toxin. These weak interactions mentioned to occur during the first minutes can also be seen for the CNF aerogel, where some adsorption is presented but is quickly lost to instead adsorb water in these used active points on the surface.



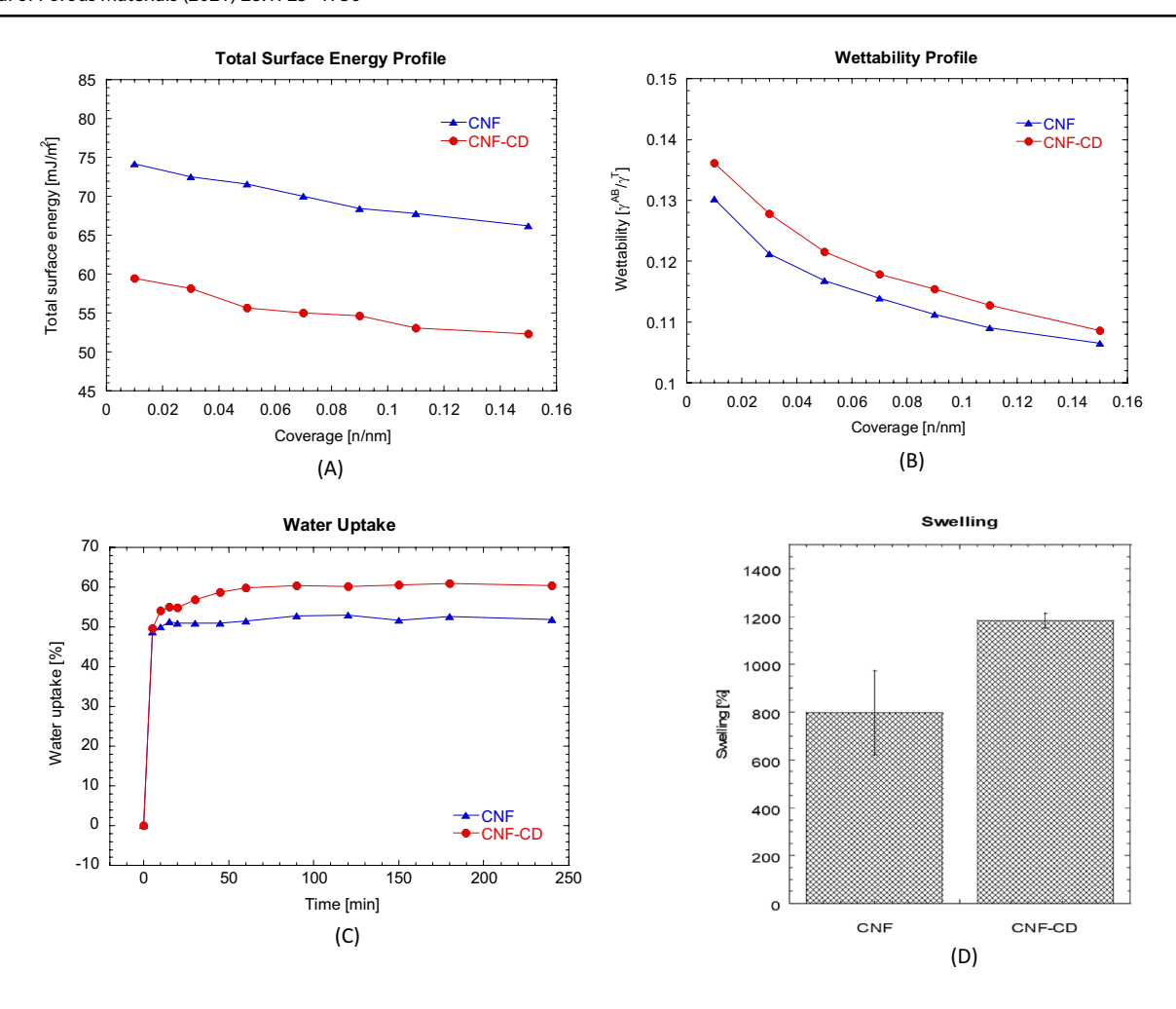


Fig. 4 Comparison between on surface energy a, wettability b, water uptake c, and swelling d of the aerogels obtained from the CNF and the modified CNF-CD

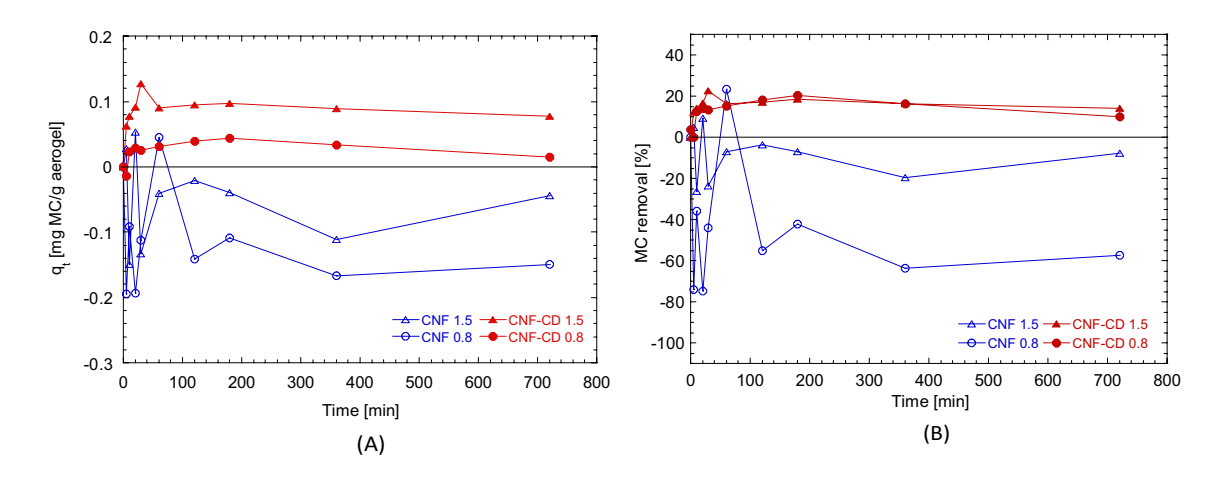


Fig. 5 Adsorption of microcystin-LR from solutions with concentrations 0.8 and 1.5 μ g/mL by aerogels prepared with CNF and CNF-CD presented in ${\bf a}$ adsorption capacity [mg/g] and ${\bf b}$ removal percentage [%]



Table 3 Parameters for adsorption of microcystin-LR (MC) and methylene blue (MB) by aerogel filters

Adsorption system		Pseudo-first order		Pseudo-second order			
Sorbent	Adsorbate	qe (mg/g)	k ₁ (min ⁻¹)	\mathbb{R}^2	qe (mg/g)	k ₂ (g/mg min)	\mathbb{R}^2
CNF	MC 1.5	N.A	N.A	N.A	-0.047	10.678	0.8603
	MC 0.8	N.A	N.A	N.A	-0.143	0.2370	0.8781
	MB	9.086	0.0024	0.9439	10.51	0.0004	0.9760
CNF-CD	MC 1.5	N.A	N.A	N.A	0.078	1.048	0.9947
	MC 0.8	N.A	N.A	N.A	0.034	8.211	0.9789
	MB	3.463	0.0023	0.9474	3.935	0.1050	0.8920

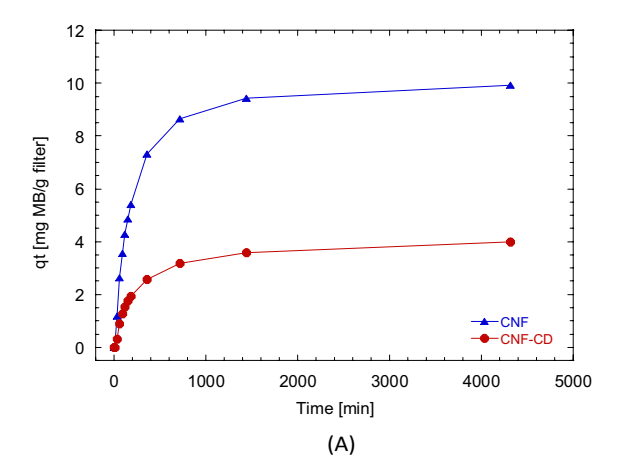
Regarding the fitting into a pseudo-first-order, as the adsorption capacity was never in total equilibrium, which in turn made some of the values obtained after the difference to have negative values. These negative values do not have a real logarithm value, making the fitting unviable. However, using the chemical theoretical universal rate law for kinetic reactions logic, from which these pseudo models are based [53], the second-order should consider the first level as a factor in the progressive addition [54, 55].

In the case of adsorption of methylene blue (MB) (Fig. 6a), the fitted maximum adsorption capability in equilibrium for CNF filters was 203% higher in the case of pristine CNF when compared to CNF-CD. As suggested by the different nature of the pollutants, the main difference in this behaviour may relate to the different adsorption mechanisms involved. In the case of microcystin-LR, the target for the adsorption is the hydrophobic Adda group, while in the case of MB, the interaction with the CNF aerogels is mainly with the partially charged nitrogen present at both ends of the dye molecule. Finally, when the desorption of MB was followed (Fig. 6b), the CNF-CD released up to 42% of the adsorbed load after 24 h (1440 min), while the CNF released only

14% over that time. This further confirms that the interactions between the CNF and the MB were stronger than the CNF-CD and MB.

Overall, this difference in adsorption capacity -with a higher capturing of the MB into CNF- can be related to the higher surface energy of the material as discussed in Sect. Aerogel formation, caused by the higher number of charged points on the surface of the CNF aerogels. As electrostatic interactions -including polar charged interactions and dispersive forces- are the main driving force in the adsorption of charged molecules like MB onto cellulose, this is predominantly favourable for pristine CNF aerogels [30]. Meanwhile, adsorption into CNF-CD surface needs a different driving force, which is mainly hydrophobic due to the cavities available with the immobilized cyclodextrin, just as observed with the preferent adsorption of the microcystin-LR, and seen on the model surfaces [39].

Overall, these adsorption experiments prove the capacity of the CNF-CD to capture and remove pollutants with short residency times. However successful, the process by which the aerogels were formed came with a high loss of surface area compared with other aerogels that had BET surface area tenfold higher [56]. A change in the fabrication approach could increase the surface area of the nanofibrils that is kept while structuring, which would consequently increase their



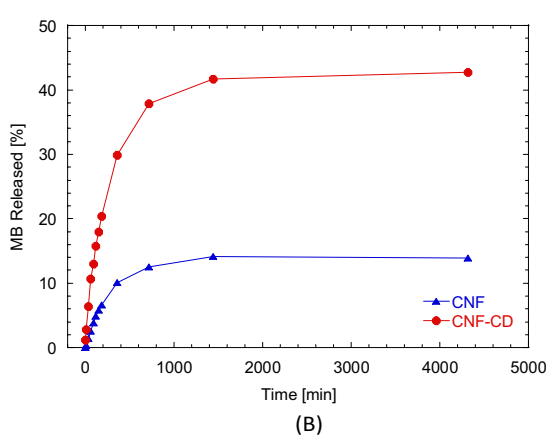


Fig. 6 a Adsorption and b desorption of methylene blue (MB) from a 15 mg/L solution by aerogels prepared with CNF and CNF-CD



capacity to capture pollutants, therefore enhancing the benefits of these bio-based adsorbents.

4 Conclusions

In this work, wood derived cellulose nanofibrils were successfully decorated with β -cyclodextrin, which were then used to form aerogels by solvent exchange and freezedrying. These CNF-CD aerogels resulted in materials with lower surface area, porosity, and surface energy than those generated from pure cellulose nanofibrils. However, their water uptake, swelling and wettability was increased due to the increase in energetically available points with the cyclodextrin and the epichlorohydrin bridges. Furthermore, this work aims to understanding the surface chemistry and properties of these type of systems to better comprehend the interactions between CNF-CD co-polymers with molecules and pollutants to further improve bio-based water filtration systems.

Consequently, when the studied aerogels were tested for adsorption of selected pollutants, those made of CNF-CD showed higher adsorption of aromatic components such as microcystin-LR, driven by thermodynamic interactions. In the case of pristine CNF aerogels, adsorption of methylene blue was preferred, predominantly driven by electrostatic forces, as more polar residues were present in the structure. Therefore, this work sets a precedent on the potential use of cellulose nanofibril grafted with cyclodextrin on the formation of porous aerogels for removal of water contaminants. As expected, limitations regarding surface area available for adsorption mechanisms was impaired due to solvent exchange/freeze drying processes, further work on preserving the aerogels surface area is anticipated to improve the performance of bio-based materials to remove multiple types of pollutants from water sources.

Supplementary Information The online version contains supplementary material available at https://doi.org/10.1007/s10934-021-01109-w.

Acknowledgements This work was supported by the USDA National Institute of Food and Agriculture, Hatch program (ALA013-17003) and McIntire-Stennis program (1022526). The School of Forestry and Wildlife Sciences at Auburn University's financial support to complete this work is much appreciated. The authors would like to acknowledge Vivek Patil and the Bioenergy Center of Auburn University for the access and help to the thermogravimetric analysis. This work made use of Aalto University Bioeconomy Facilities, the FinnCERES – Competence Centre for the Materials Bioeconomy support is highly appreciated. The authors also want to acknowledge Dr. Michael Bortner and Eric Gilmer from Virginia Tech for their help to perform the ICP experiments.

Data availability The data that support the findings of this study are available from the corresponding author upon reasonable request.

Declarations

Conflict of interest The authors declare no conflict of interest to this work

References

- 1. World Health Organization, WHO (2017).
- 2. United Nations, UN Water (n.d.).
- 3. United Nations Department of Economic and Social Affairs, (2014).
- Á. Piñeiro, X. Banquy, S. Pérez-Casas, E. Tovar, A. García, A. Villa, A. Amigo, A.E. Mark, M. Costas, J. Phys. Chem. B 111, 4383 (2007)
- J. Lee, H.W. Walker, Colloids Surfaces A Physicochem. Eng. Asp. 373, 94 (2011)
- 6. N. Lin, A. Dufresne, Biomacromol 14, 871 (2013)
- 7. I. Ali, Chem. Rev. **112**, 5073 (2012)
- A.W. Carpenter, C.F. de Lannoy, M.R. Wiesner, Env. Sci Technol. 49, 209 (2015)
- S.K. Papageorgiou, F.K. Katsaros, E.P. Favvas, G.E. Romanos, C.P. Athanasekou, K.G. Beltsios, O.I. Tzialla, P. Falaras, Water Res. 46, 1858 (2012)
- D. Gomez Maldonado, I.B. Vega Erramuspe, M.S. Peresin, BioResources 14, 10093 (2019)
- A.W. Carpenter, C.-F. de Lannoy, M.R. Wiesner, Environ. Sci. Technol. 49, 5277 (2015)
- H.A. Devrimci, A.M. Yuksel, F.D. Sanin, Desalination 299, 16 (2012)
- 13. D. Zeng, J. Wu, J.F. Kennedy, Carbohydr. Polym. 71, 135 (2008)
- M. Vakili, S. Deng, G. Cagnetta, W. Wang, P. Meng, D. Liu, G. Yu, Sep. Purif. Technol. 224, 373 (2019)
- K. Missoum, M.N. Belgacem, J. Bras, Materials (Basel). 6, 1745 (2013)
- K.Y. Lee, F. Quero, J.J. Blaker, C.A.S. Hill, S.J. Eichhorn, A. Bismarck, Cellulose 18, 595 (2011)
- P. Kumar Dutta, J. Dutta, V.S. Tripathi, J. Sci. Ind. Res. 63, 20 (2004)
- 18. H. Sixta, Handbook of Pulp (Wiley Online Library, 2006)
- K. Oksman, A. P. Mathew, A. B. Pia Qvintus, O. Rojas, and M. Sain, Handbook of Green Materials, Bionanomaterials: Separation Processes, Characterization and Properties Vol.5 (2014)
- M.C. Iglesias, D. Gomez-Maldonado, B.K. Via, Z. Jiang, M.S. Peresin, For. Prod. J. 70, 10 (2020)
- 21. L. Jin, Q. Sun, Q. Xu, Y. Xu, Bioresour. Technol. 197, 348 (2015)
- T. Ristić, T. Mohan, R. Kargl, S. Hribernik, A. Doliška, K. Stana-Kleinschek, L. Fras, Cellulose 21, 2315 (2014)
- H. Orelma, I. Filpponen, L.-S. Johansson, J. Laine, O.J. Rojas, Biomacromol 12, 4311 (2011)
- M.S. Toivonen, A. Kaskela, O.J. Rojas, E.I. Kauppinen, O. Ikkala, Adv. Funct. Mater. 25, 6618 (2015)
- H. Sehaqui, Q. Zhou, L.A. Berglund, Compos. Sci. Technol. 71, 1593 (2011)
- L. V. A. Gurgel, O. K. Júnior, R. P. de F. Gil, and L. F. Gil, Bioresour. Technol. 99, 3077 (2008)
- A. Kardam, K.R. Raj, S. Srivastava, M.M. Srivastava, Clean Technol. Environ Policy 16, 385 (2014)
- R. Koshani, A. Madadlou, Trends Food Sci. Technol. 71, 268 (2018)
- V.S. Raghuwanshi, J. Su, C.J. Garvey, S.A. Holt, P.J. Holden, W.J. Batchelor, G. Garnier, Biomacromol 18, 2439 (2017)
- 30. S. Lombardo, W. Thielemans, Cellulose 26, 249 (2019)
- 31. A. Sinha, N.R. Jana, A.C.S. Appl, Mater. Interfaces 7, 9911 (2015)



- L. Fan, C. Luo, M. Sun, H. Qiu, X. Li, Colloids Surfaces B Biointerfaces 103, 601 (2013)
- P. Chen, H.W. Liang, X.H. Lv, H.Z. Zhu, H. Bin Yao, S.H. Yu, ACS Nano 5, 5928 (2011)
- 34. S. Kim, Y.S. Yun, Y.E. Choi, Bioresour. Technol. 247, 690 (2018)
- 35. C. Dong, L.Y. Qian, G.L. Zhao, B.H. He, H.N. Xiao, Mater. Lett. **124**, 181 (2014)
- A. Celebioglu, S. Demirci, T. Uyar, Appl. Surf. Sci. 305, 581 (2014)
- T.F.G.G. Cova, D. Murtinho, A.A.C.C. Pais, A.J.M. Valente, Front. Chem. 6, 271 (2018)
- 38. L. Zhang, J. Zhou, L. Zhang, Carbohydr. Polym. 94, 386 (2013)
- D. Gomez-Maldonado, I.B. Vega Erramuspe, I. Filpponen, L.-S. Johansson, S. Lombardo, J. Zhu, W. Thielemans, M.S. Peresin, Polymers (Basel). 11, 2075 (2019)
- E. Espinosa, Q. Tarrés, M. Delgado-Aguilar, I. González, P. Mutjé, A. Rodríguez, Cellulose 23, 837 (2016)
- L. Johansson, J. M. Campbell, and O. J. Rojas, Surf. Interface Anal. 1 (2020)
- 42. D. Briggs, G. Beamson, Anal. Chem. 65, 1517 (1993)
- 43. American Public Health Association and American Water Works Association and Water Environment Federation, (n.d.)
- 44. J. Meriluoto and G. A. Codd, Cyanobacterial Monitoring and Cyanotoxin Analysis (2005)
- C.D. Tran, S. Duri, A. Delneri, M. Franko, J. Hazard. Mater. 253, 355 (2013)
- D.J. Mozdyniewicz, K. Nieminen, H. Sixta, Cellulose 20, 1437 (2013)

- N. Morin-Crini, P. Winterton, S. Fourmentin, L.D. Wilson, É. Fenyvesi, G. Crini, Prog. Polym. Sci. 78, 1 (2018)
- I.A. Udoetok, R.M. Dimmick, L.D. Wilson, J.V. Headley, Carbohydr. Polym. 136, 329 (2016)
- B. Medronho, R. Andrade, V. Vivod, A. Ostlund, M.G. Miguel,
 B. Lindman, B. Voncina, A.J.M. Valente, Carbohydr. Polym. 93, 324 (2013)
- C. Dong, Y. Ye, L. Qian, G. Zhao, B. He, H. Xiao, Cellulose 21, 1921 (2014)
- R. Ajdary, B. L. Tardy, B. D. Mattos, L. Bai, and O. J. Rojas, Adv. Mater. 2001085 (2020)
- A.S. Archimandritis, T. Papadimitriou, K.A. Kormas, C.S. Laspidou, K. Yannakopoulou, Y.G. Lazarou, Sustain. Chem. Pharm. 3, 25 (2016)
- Y. Liu, Colloids Surfaces A Physicochem. Eng. Asp. 320, 275 (2008)
- F.C. Wu, R.L. Tseng, S.C. Huang, R.S. Juang, Chem. Eng. J. 151, 1 (2009)
- 55. J. Lin, L. Wang, Front. Environ. Sci. Eng. China 3, 320 (2009)
- 56. L.Y. Long, Y.X. Weng, Y.Z. Wang, Polymers (Basel). 8, 1 (2018)

Publisher's Note Springer Nature remains neutral with regard to jurisdictional claims in published maps and institutional affiliations.

